ANALYSIS AND CONTROL OF BIFURCATION IN PERMANENT MAGNET DC MOTOR DRIVE

Bharathi.S.B
Department of EEE, K.L.N College of Information Technology,
Sivagangai District, Tamilnadu, India, 0452-6454167,0452-2092734,bharathisarav@gmail.com

Jessi Sahaya Shanthi.L
Department of EEE, Thiagarajar College of Engineering,
Madurai, Tamilnadu, India, ljseee@tce.edu

Abstract: *In this paper, period doubling bifurcation of a Permanent Magnet Direct Current (PMDC) motor is identified mathematically using Poincare map and Floquet theory or Monodromy matrix method. Derivative of the Poincare map gives Jacobian matrix (J-matrix) and Floquet theory calculates Monodromy matrix (M-matrix). The period doubling operation is identified when one of the eigen values of the matrix exceeds unity along the negative real axis. Poincare map identifies the period doubling bifurcation for various parametric conditions and the results obtained agrees with results of the Monodromy matrix method. In this work, calculation of eigen values is performed with J-matrix and compared with M-matrix under various proportional gains, supply voltages and load torques. Also the numerical calculation is verified by means of MATLAB Simulink outputs of speed and current waveform. In order to control the bifurcation behavior, an Extended Time Delay Auto Synchronization (ETDAS) controller is used. This controller controls bifurcation and extends the normal period-1 operation of the drive. This analysis is useful in identifying the stable operating region of the system. Also period doubling operation further leads to chaotic behaviour, the controller helps to avoid such chaos in the operation of the drive system.*

Keywords: *Bifurcation, Chaos, Eigen value, ETDAS, PMDC, Poincare map, Monodromy matrix.*

1. Introduction

Nowadays due to the increasing air pollution, electric vehicles (EVs) and hybrid electric vehicles (HEVs) are becoming popular. Large rating PMDC drive is preferred in some HEVs. In some vehicles, small rating PMDC motors are used in operating the wiper system. So analyzing the PMDC motor is essential while considering EVs. When operating the electric vehicle, it is necessary to change the speed, load and some other parameters of the drive system. In some varying parametric conditions, irregular chaotic vibrations are produced in the motor drive system. These unwanted vibrations create safety hazards to the vehicle and also disturbance to the driver. In such conditions the small wiper motor also experiences vibration and jerks. In this paper, chaos present in the PMDC drive is identified. If a chaotic controller is included in the system, stability can be improved.

Electric drives are usually operated by power electronic switching devices and are more prone to nonlinearity and hence show chaotic behavior in its operation [1]. All the real life problems can only be modeled by nonlinear systems. Nonlinear phenomena and computation of Poincare map are studied [2]. Different analysis methods to find out bifurcation, chaos and subharmonics occurring in DC motor drive are discussed here. Eigen value analysis is performed to identify the dynamic bifurcation occurring in a current mode controlled DC chopper fed PMDC drive [3]. Chaos developed through quasi periodic orbits is detailed in a voltage mode and current mode controlled DC drive [4]. Analysis and compensation of chaos in DC motor drive are also studied in [5]. Coexistence of period-1 and period-3 behavior of a DC drive operated by a full bridge converter is identified using Monodromy matrix method [6]. Analysis of bifurcation and chaos in DC motor drive is reported in [7]. Anti-control of chaos in PMDC motor is performed in vibratory compactors [8]. Modeling of sub harmonic and chaotic behavior in DC drives is performed [9]. Equivalent circuit based analysis of chaos is explained for a DC motor [10]. Sub harmonics and chaos analysis for switched reluctance motors are presented in [11].

Chaos present in an automotive wiper system is identified by means of Poincare map, time responses and frequency spectra [12]. The work stated in [13] considered a BLDC motor for the synchronization of chaos. Chaos identified in a PMSM is controlled using non-linear feedback control method [14]. ETDAS control of automotive wiper system operated by a PMDC

motor is analyzed [15]. Monodromy matrix and eigen value are derived for PMDC and SRM and the period doubling bifurcation is identified [16]. Various chaos control, anti control and synchronization methods are discussed [17-20].

In the present work, both J-matrix and M-matrix of the PMDC model are derived in a step by step manner. The parameters considered here for variation are proportional gain, supply voltage and load torque. Then the eigen values of the matrices are tabulated for comparison. This numerically identified bifurcation is observed in simulation also using MATLAB simulink. Phase plots are also drawn to confirm the existence of period doubling bifurcation. Finally to control the bifurcation and to extend the normal periodic operation, ETDAS controller is introduced in the simulation work. Output speed and current waveforms are presented with and without controller.

2. Modeling of PMDC motor

Fig.1 shows the block schematic diagram of a closed loop PMDC drive considered in this paper. DC Supply voltage (V_{in}) is given to the Chopper. The motor is supplied by the DC-DC chopper which gives controlled DC output voltage. The controlled DC output from the chopper can be obtained by means of operating it using a PWM generator. PWM generation is based on the magnitudes of ramp (V_{ramp}) and control signals (V_{con}) [3].Control signal (V_{con}) is the difference between actual and reference speed amplified by a proportional controller with gain K_p. It is expressed as,

$$V_{con}(t) = K_p(\omega_{ref} - \omega(t))$$

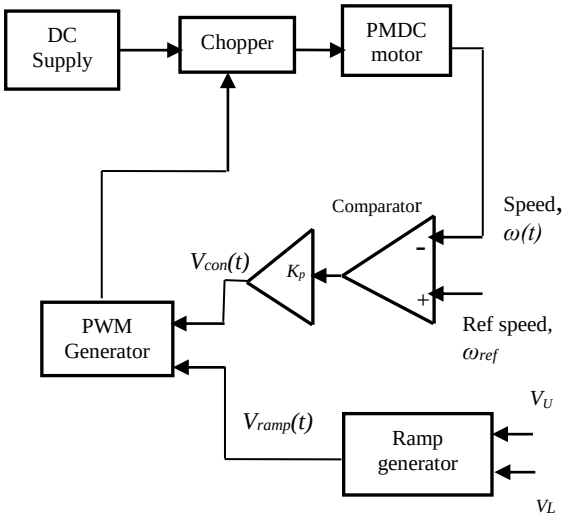

Fig. 1. Block diagram for PMDC motor drive

Ramp signal (V_{ramp}) is generated in a ramp generator and it is compared with the control signal for the generation of PWM pulses. Ramp voltage is expressed as,

$$V_{ramp}(t) = V_L + (V_U - V_L)\frac{t}{T}$$

Here V_L and V_U are the lower and upper thresholdvoltages of the ramp signal expressed in volts. *T*-is the total time period of ramp signal in seconds.

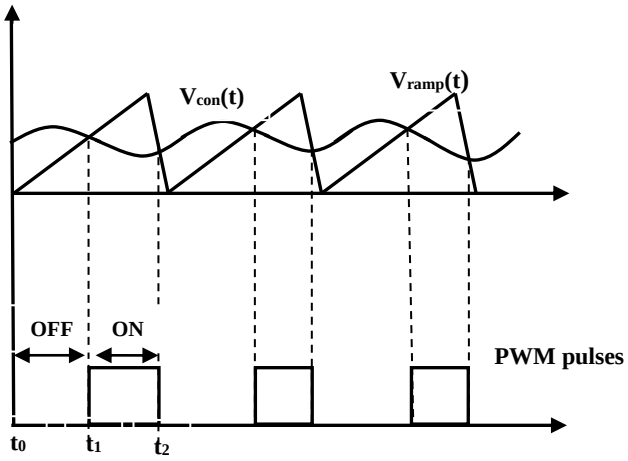

Fig. 2.Generation of PWM pulses

When $V_{ramp} > V_{con}$, pulses are applied to the chopper switch to turn ON. When $V_{ramp} < V_{con}$, pulses are not applied to the chopper switch and turned OFF. Fig.2 shows the comparison of control and ramp voltages and PWM pulses generated. In this manner, the closed loop drive performs voltage mode controlled DC motor operation [9].

The PMDC motor supplied by a voltage mode controlled chopper with a proportional controller can be represented by a state space model [9].The state variables are, $X(t) = \begin{bmatrix} \omega(t) \\ i(t) \end{bmatrix}$

Where,
ω- speed of the motor in rad/ sec
i- motor phase current in amperes

During switch ON ($V_{ramp} > V_{con}$) the state equation is,

$$\begin{bmatrix} \frac{d\omega(t)}{dt} \\ \frac{di(t)}{dt} \end{bmatrix} = \begin{bmatrix} -\frac{B}{J} & \frac{K_t}{J} \\ -\frac{K_e}{L} & -\frac{R}{L} \end{bmatrix} \begin{bmatrix} \omega(t) \\ i(t) \end{bmatrix} + \begin{bmatrix} -\frac{T_L}{J} \\ \frac{V_{in}}{L} \end{bmatrix} \quad (1)$$

The state matrix is common for both the ON and OFFstate of operation and is given by,

$$A=\begin{bmatrix} -\frac{B}{J} & \frac{K_t}{J} \\ -\frac{K_e}{L} & -\frac{R}{L} \end{bmatrix}$$

Here,
B- friction coefficient in Nm-sec/rad;
J-inertia in Nm-sec^2/rad;
K_t-torque constant in Nm/A;
K_e-EMF constant in V-sec/rad;
R-winding resistance in Ω;
L-winding inductance in H;
T_L-load torque in Nm;

The above equation means that the supply voltage circulates current through the phase winding of the motor.

When the switch is turned OFF ($V_{ramp} < V_{con}$), the state equation is as given below. There is no supply current but the current flows due to inductive effect through the freewheeling diode [12].

$$\begin{bmatrix} \frac{d\omega(t)}{dt} \\ \frac{di(t)}{dt} \end{bmatrix}=\begin{bmatrix} -\frac{B}{J} & \frac{K_t}{J} \\ -\frac{K_e}{L} & -\frac{R}{L} \end{bmatrix}\begin{bmatrix} \omega(t) \\ i(t) \end{bmatrix}+\begin{bmatrix} -\frac{T_L}{J} \\ 0 \end{bmatrix} \quad (2)$$

3. Methodology used in the analysis

In this paper, two different analytical methods called Poincare map and Monodromy matrix method are discussed. In Poincare map, a switching surface is considered where switching of the power converter operating the motor is performed. This means that the switching surface separates the ON and OFF states of the DC chopper. This surface is considered as the Poincare plane. This mapping technique checks the flow of the system state variables across the surface. Each crossing across the plane is considered as a point. If a state variable is periodic with period 'T', the instantaneous state of the variable for one complete period (T) gives a set of crossing points. On connecting these points, a state trajectory is obtained. Solution of the state equation is used to find the trajectory of each state variable at every instant of time. Using the solution, this mapping function derives the present state of the system variable in terms of its past state. Differentiating the mapping function gives Jacobian matrix. Eigen value calculated for this Jacobian matrix determines the system's bifurcation condition. Among the many types of bifurcation methods, period doubling or flip bifurcation is considered here.

The second method discussed in this paper is the Monodromy matrix method in which solution of state equation is used. The Poincare map calculates the system behavior during the flow of the state around the trajectory but the transition from one state to other state is not included. This method includes not only the system behavior during flow of the trajectory in one particular state but also the transition from one state to other.Eigen values are found out for the Monodromy matrix to show the bifurcation point. Using both these methods, flip or period doubling bifurcation is confirmed.

These results help in improving the performance of a particular drive system by avoiding the bifurcation conditions in sensitive applications like servo motors, robots, etc. Also the methods can be extended to any drive system for analysis if the state equations are known.In the following sections, both the methods are explained under various operating conditions.

A. Poincare map

A detailed analysis of Poincare map based derivation of J-matrix and stability analysis are carried out in this section. To perform Poincare map in the above model, solution of the state equation is to be found [3]. The total time period is divided into two intervals including OFF-time (t_0 to t_1) and ON-time (t_1 to t_2). Solving the state equation (2) during OFF-time (t_0 to t_1),

$$X(t_1)=\phi(t_1-t_0)X(t_0)+\int_{t_0}^{t_1}\phi(t_1-\tau)V_2\,d\tau \quad (3)$$

Here,
$X(t_0)=\begin{bmatrix} \omega(t_0) \\ i(t_0) \end{bmatrix}$ isthe initial state of the system and
$V_2=\begin{bmatrix} -\frac{T_L}{J} \\ 0 \end{bmatrix}$.

Substituting $\phi(t_1-t_0)=e^{A(t_1-t_0)}$ in equation (3) and integrating the second term,

$$X(t_1)=-A^{-1}V_2+e^{A(t_1-t_0)}(X(t_0)+A^{-1}V_2) \quad (4)$$

Similarly the solution of equation (1) during the interval (t_1, t_2) is,

$$X(t_2) = \phi(t_2 - t_1) X(t_1) + \int_{t_1}^{t_2} \phi(t_2 - \tau)\, V_1 \, d\tau \qquad (5)$$

Here $X(t_1)$ is calculated from equation (4). Substituting $\phi(t_2 - t_1) = e^{A(t_2 - t_1)}$ and $V_1 = \begin{bmatrix} -\frac{T_L}{J} \\ \frac{V_{in}}{L} \end{bmatrix}$ in equation (5) and integrating the second term,

$$X(t_2) = -A^{-1}V_1 + e^{A(t_2 - t_1)}(X(t_1) + A^{-1} V_1) \qquad (6)$$

Generalizing equations (4) and (6),

$$X(t) = -A^{-1}V_k + e^{A(T - t_0)}(X(t_0) + A^{-1} V_k)$$

where, V_k (for k=1 or 2) is the input vector depends on whether switch is ON or OFF and $X(t_0)$ is the initial state vector at t=t_0.The final solution $X(t_2)$ is a function of the initial state $X(t_0)$. Using the above general equation, Poincare map of the drive system is derived for any state m. State$(m+1)$ is expressed as the mapping function of m^{th} state of the system as,

$$X_{m+1} = P(X_m) \qquad (7)$$

The map $P(X_m)$ given in equation (7) is divided into two portions as per the switch operation. During the first interval $(t = t_0 \text{ to } t_1)$, the state variable changes its state from $X(t_0)$ to $X(t_1)$. Here $t_1$is the time equal to δ times the total time i.e., $t_1 = \delta T$, where $(\delta = 1-d)$; d-duty ratio. And in the second part of the total period ($t = t_1 \text{ to } t_2$), the state variable changes its state from $X(t_1)$ to $X(t_2)$. So the mapping function in equation (7) can be expressed as,

$$X(t_1) = P(X(t_0)) \text{ and } X(t_2) = P(X(t_1)) \qquad (8)$$

Therefore,

$$X(t_2) = -A^{-1}V_1 + e^{A(t_2 - t_1)}\left(X(t_1) + A^{-1}V_1\right)$$

$$X(t_1) = -A^{-1}V_2 + e^{A(t_1 - t_0)}\left(X(t_0) + A^{-1}V_2\right)$$

Substituting $X(t_1)$ expression in $X(t_2)$,

$$X(t_2) = -A^{-1}V_1 + e^{A(t_2 - t_1)}\left(-A^{-1}V_2 + e^{A(t_1 - t_0)}\left(X(t_0) + A^{-1}V_2\right) + A^{-1}V_1\right) \qquad (9)$$

$$X(t_2) = -A^{-1}V_1 - e^{A(t_2 - t_1)}A^{-1}V_2 + e^{A(t_2 - t_0)} X(t_0) + e^{A(t_2 - t_0)} A^{-1}V_2 + A^{-1}V_1 e^{A(t_2 - t_1)} \qquad (10)$$

After simplification,

$$X(t_2) = P(X(t_0)) = -A^{-1}V_1 + e^{A(t_2 - t_0)}(X(t_0) + A^{-1}V_2) + e^{A(t_2 - t_1)}A^{-1}(V_1 - V_2) \qquad (11)$$

The Poincare map is obtained by the above equation from which the state equation at the second state is expressed as a function of the initial state. Differentiating the above mapping function,

$$DP(X(t_0)) = e^{A(t_2 - t_0)} - e^{A(t_2 - t_1)}(V_1 - V_2)t_2 \frac{d\delta}{dX(t_0)} \qquad (12)$$

The switching surface [9] is defined as,

$$h(t_1) = \left[K_p\ 0\right]\left(-A^{-1}V_2 + e^{A(t_1 - t_0)}\left(X(t_0) + A^{-1}V_2\right)\right) - \left[\omega_{ref}\ 0\right] - V_{ramp}(\delta T) \qquad (13)$$

To find $\frac{d\delta}{dX(t_0)}$, the switching hyper surface expression in equation (13) is used.

Now,

$$\frac{dh}{dX(t_0)} = -\frac{dh}{d\delta}\frac{d\delta}{dX(t_0)} \qquad (14)$$

Therefore,

$$\frac{d\delta}{dX(t_0)} = \left(\frac{dh}{d\delta}\right)^{-1}\frac{dh}{dX(t_0)}$$

$$\frac{d\delta}{dX(t_0)} = -\left(\left[K_p\ 0\right] e^{A(t_1 - t_0)}\left(X(t_0) + A^{-1}V_2\right)At_2 - (V_U - V_L)\right)^{-1}\left[K_p\ 0\right] e^{A(t_1 - t_0)} \qquad (15)$$

Substituting equation (15) in equation (12) and expanding the matrices,

$$DP(X(t_0)) = e^{A(t_2 - t_0)} + e^{A(t_2 - t_1)}(V_2 - V_1)t_2\left(-\left(\left[K_p\ 0\right] e^{A(t_1 - t_0)}\left(AX(t_0) + V_2\right)t_2 - (V_U - V_L)\right)^{-1}\right)\left[K_p\ 0\right] e^{A(t_1 - t_0)} \qquad (16)$$

Equation (16) gives the 2x2 matrix which is the Jacobian matrix, J. The initial state vector $X(t_0)$ is unknown in this equation. Since the solution is periodic, $X(t_2)=X(t_0)$. Using this condition in equation (10),

$$X(t_0) = -A^{-1}V_1 - e^{A(t_2 - t_1)}A^{-1}V_2 + e^{A(t_2 - t_0)} X(t_0) + e^{A(t_2 - t_0)} A^{-1}V_2 + A^{-1}V_1 e^{A(t_2 - t_1)} \qquad (17)$$

Simplifying,

$$X(t_0) = (I - e^{A(t_2 - t_0)})^{-1}(-A^{-1}V_1 - e^{A(t_2 - t_1)}A^{-1}V_2 + e^{A(t_2 - t_0)} A^{-1}V_2 + A^{-1}V_1 e^{A(t_2 - t_1)}) \qquad (18)$$

where, I-identity matrix (2x2).

Substituting equation (18) in equation (13), the equation for switching surface is obtained only in terms of δ. Now solving the switching surface equation using Newton Raphson method, the value of δ is obtained. Then t_1 can be calculated from $t_1=\delta T$ (where total time,$T=t_2$, and initial time, $t_0=0$). Substituting δ value in equation (18) gives the initial state vector $X(t_0)$ to be substituted in equation (16) to find the J-matrix. The above procedure is given in the flow diagram in Fig. 3.

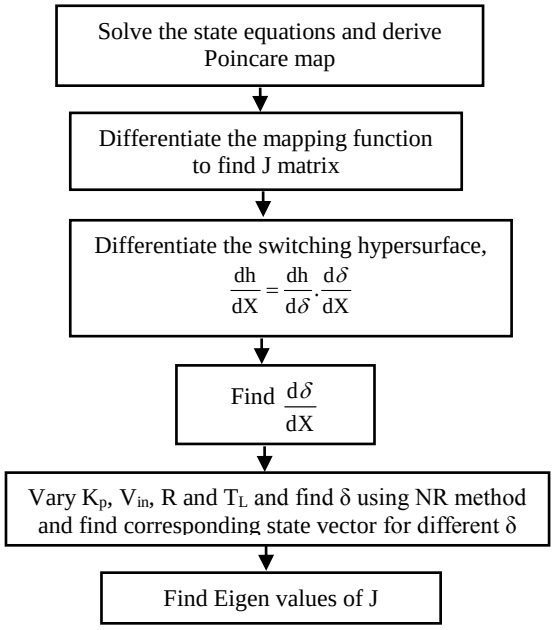

Fig. 3. Flow diagram for Poincare map

B. Monodromy matrix approach

To find the stability, the Monodromy matrix is calculated around the trajectory of the system state. The matrix explaining the flow of the trajectory in one particular state is called saltation matrix, *S* and the matrix determining the transition operation is named state transition matrix, *Φ*. To find out the entire operation of the system during one complete cycle, the saltation matrix and state transition matrix must be multiplied which becomes Monodromy matrix, *M*.

$$M = S_2 \times \phi_2 \times S_1 \times \phi_1 \tag{19}$$

Here, S_2, S_1 are the saltation matrices and ϕ_2, ϕ_1 are the state transition matrices for the OFF and ON states respectively. The saltation matrix S_1 can be expressed as,

$$S_1 = \begin{bmatrix} 1 & 0 \\ S_{21} & 1 \end{bmatrix} \tag{20}$$

Here,

$$S_{21} = \frac{\frac{V_{in}}{L}}{\left(\frac{K_t X_2(t_1) - BX_1(t_1) - T_L}{J}\right) - \frac{V_U - V_L}{T}} \tag{21}$$

The second saltation matrix S_2 is given by,

$$S_2 = \begin{bmatrix} 1 & 0 \\ 0 & 1 \end{bmatrix} \tag{22}$$

The state transition matrices are given by,

$$\phi_1 = e^{A(t_1 - t_0)} \tag{23}$$

$$\phi_2 = e^{A(t_2 - t_1)} \tag{24}$$

Substituting equations (20) to (24) in equation (19), the Monodromy matrix (2x2 matrix) is obtained.

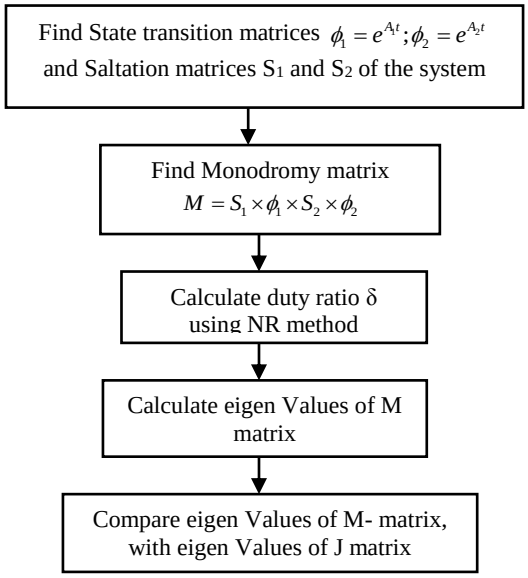

Fig.4. Flow diagram for Monodromy matrix method

Fig.4 explains the procedure involved in this Monodromy matrix method.

4. Control method and improvement of stability

To improve the performance of the drive and to avoid bifurcation, a controller has to be incorporated in the circuit. The control action must provide stable operation of the drive system even for varying parameter conditions. The time delayed feedback control (TDFC) and extended time-delay auto-synchronization (ETDAS) control are two methods that follow time delay feedback

technique. Both these feedback controls compare the present and previous states of the feedback signal [12]. If there exists a difference in the two states of the signal due to bifurcation, control action is applied. If there is no such behavior and the system works under normal periodic operation, there is no difference found in the comparison and the control action is not necessary. Thus the controller maintains the normal period-1 stable operation by means of comparison and control action.

Among the two methods, ETDAS is found better and is incorporated here. So in this paper the results obtained after including ETDAS controller are also presented.

4.1 ETDAS control

Extended time-delay auto-synchronization (ETDAS) is applied for a DC drive system and stabilization is achieved in [12]. Speed feedback **ω**(t)of the PMDC model is taken as the input to the controller. As per the principle of ETDAS controller, F(t) is the perturbation term added to V_{con}(t) and the expressions are presented in equation (25) and (26).

$$F(t) = K\left[(1-R_c)\sum_{q=1}^{\infty} R_c^{\,q-1}\omega(t-q\tau) - \omega(t)\right] \qquad (25)$$

$$V_{con}^{\,*}(t) = F(t) + V_{con}(t) \qquad (26)$$

Where R_c is the regressive parameter that ranges from 0 to 1.

Fig.5 explains the ETDAS control logic applicable for the PMDC drive system. A time delay(τ) is included in the speed output of the motor **ω**(t), before it enters into the comparator. After the inclusion of the controller in the PMDC drive, the output waveforms are given in the subsequent sections. When a periodic signal x(t) with period 'T' undergoes period doubling, the period of oscillation becomes '2T'. At this condition, the difference x(t-τ)-x(t) is calculated in the controller which produces the error between the period-1 and period-2 signals.

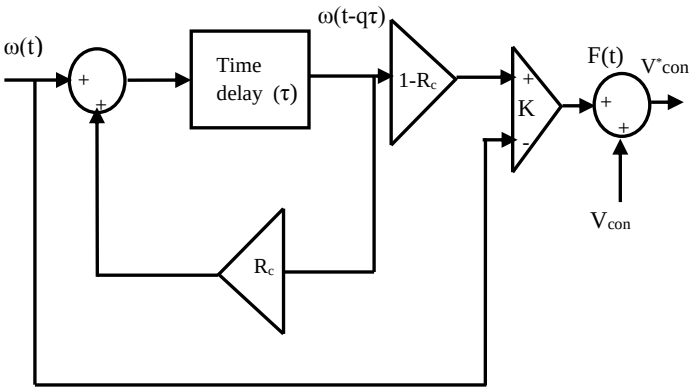

Fig 5. ETDAS control logic

The error is controlled by proper selection of controller gain 'K'. The controlled output F(t) is added with the original signal to reduce the error value. The control action is repeated infinite times in the controller until the error is completely eliminated. This means that the period doubled waveform becomes period-1 after control. So by proper selection of time delay 'τ' value and gain 'K' value, we can make the signal to oscillate in the desired period. Period doubling will get eliminated. Now there is no control required and the control action becomes zero.

Time delay (τ) of 0.01 second, K=0.1 and R_c=0.85 are used here. Now the same parameter variations are carried out after the inclusion of controller.

5. Simulation Results

In this section, eigen value calculated using J-matrix is compared with M-matrix and tabulated. Calculation of M-matrix for various K_p and V_{in} for the PMDC model was already presented by Nelson Okafor in his thesis [16]. In this work, both M-matrix and J-matrix are derived and numerically presented for various K_p, V_{in} and T_L. Analytical calculation of eigen values is performed using MATLAB coding (.m file). MATLAB Simulink model (.mdl) is constructed for the PMDC model.

The simulation parameters shown in table 1 are utilized for MATLAB simulation. In the subsequent sections, the results obtained from calculation and simulation waveforms are presented. For various parameter changes, speed and current output waveforms are taken.

Table 1
Simulation Parameters

S.No.	Parameter	Symbol	Value	Unit
1	Supply voltage	V_{in}	100	V
2	Winding resistance	R	3.5	Ω
3	Winding inductance	L	36	mH
4	Torque constant	K_t	0.1324	Nm/A
5	EMF constant	K_e	0.1356	V-sec/rad
6	Inertia	J	0.000971	Nm-sec^2/rad
7	Friction coefficient	B	0.000564	Nm-sec/rad
8	Load torque	T_L	0.39	Nm
9	Reference speed	ω_{ref}	100	rad/sec
10	Ramp lower level	V_L	0	V
11	Ramp higher level	V_H	2.2	V
12	Switching frequency	f	250	Hz

5.1 Effect of proportional gain K_p on Eigen values

In the PI controller used in the drive system, proportional gain is increased in response to the increase in error between the reference and actual speed. It provides a smooth control action on the system until the speed error is made zero. In this paper, speed error is processed by the PI-controller. Gain of the controller is varied to identify the bifurcation behavior.

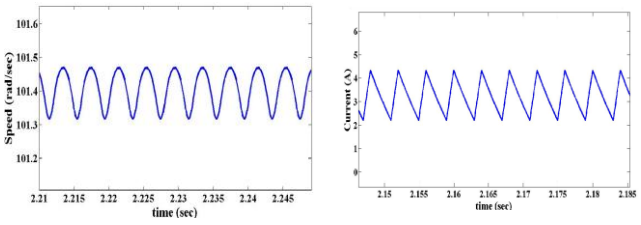

(a) (b)

Fig .6 Speed and Current output waveforms for T_L=0.39 Nm; V_{in}=100 V; R=3.5 Ω; Kp=1.2

In Fig. 6, the speed and current waveforms are periodic with period 0.004 s for K_p=1.2. Due to period doubling bifurcation at K_p=2.4, time period of these waveforms get doubled (0.008s) as observed clearly in Fig. 7. The waveforms agree with the analytical results given in table 2.
Table 2

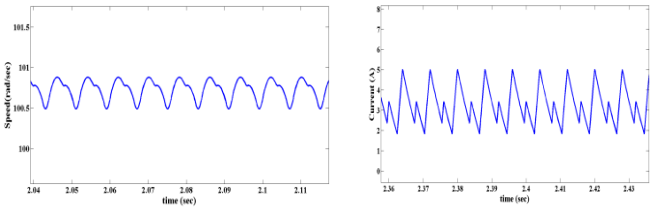

(a) (b)

Fig .7 Speed and Current output waveforms for T_L=0.39 Nm; V_{in}=100 V; R=3.5 Ω; Kp=2.4

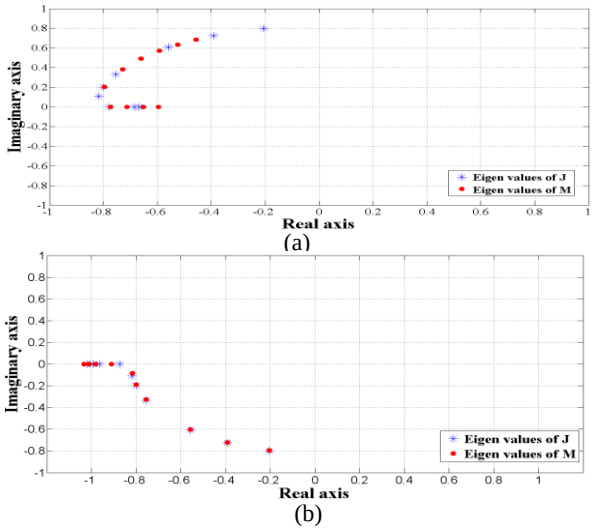

(a)
(b)

Fig. 8 Comparisons of Eigen Tracing for (a) Speed and (b) Current for various K_p values

Eigen value loci for change in proportional gain values using Poincare mapping and monodromy method are presented in fig.8. Eigen values corresponding to speed and current vectors are separately plotted in the complex plane as shown in Fig. 8 (a) and (b). Eigen values crossing (-1, 0) is clearly shown in Fig. 8(b). Any one Eigen value crossing unit circle is sufficient for the occurrence of flip bifurcation. It is seen from the tabulated values that the increase in gain value from 1.2 to 2.4 increases the eigen values along the negative real axis. At K_p=2.4, the eigen value crosses unity in the negative direction showing bifurcation behavior. It is seen that eigen values calculated using both the methods are approximately same as in table 2.

Variation of proportional gain to find bifurcation

K_p	Δ	J Matrix	Eigen values of J-matrix	M-matrix	Eigen values of M-matrix
1.2	0.7439	$\begin{bmatrix} 0.3841 & 0.2362 \\ -4.1662 & -0.7942 \end{bmatrix}$	-0.2051 + 0.7982i -0.2051 - 0.7982i	$\begin{bmatrix} 0.3841 & 0.2354 \\ -4.1661 & -0.7936 \end{bmatrix}$	-0.2048 + 0.7963i -0.2048 - 0.7963i
1.5	0.7443	$\begin{bmatrix} 0.2755 & 0.1978 \\ -4.9134 & -1.0591 \end{bmatrix}$	-0.3918 + 0.7255i -0.3918 - 0.7255i	$\begin{bmatrix} 0.2755 & 0.1969 \\ -4.9134 & -1.0585 \end{bmatrix}$	-0.3915 + 0.7230i -0.3915 - 0.7230i
1.8	0.7446	$\begin{bmatrix} 0.1786 & 0.1634 \\ -5.5812 & -1.2959 \end{bmatrix}$	-0.5586 + 0.6069i -0.5586 - 0.6069i	$\begin{bmatrix} 0.1786 & 0.1626 \\ -5.5812 & -1.2954 \end{bmatrix}$	-0.5584 + 0.6035i -0.5584 - 0.6035i
2.2	0.7449	$\begin{bmatrix} 0.0644 & 0.1229 \\ -6.3687 & -1.5752 \end{bmatrix}$	-0.7554 + 0.3324i -0.7554 - 0.3324i	$\begin{bmatrix} 0.0644 & 0.1221 \\ -6.3687 & -1.5747 \end{bmatrix}$	-0.7551 + 0.3253i -0.7551 - 0.3253i
2.3	0.7449	$\begin{bmatrix} 0.0381 & 0.1136 \\ -6.5490 & -1.6390 \end{bmatrix}$	-0.8005 + 0.2013i -0.8005 - 0.2013i	$\begin{bmatrix} 0.0380 & 0.1127 \\ -6.5489 & -1.6385 \end{bmatrix}$	-0.8002 + 0.1889i -0.8002 - 0.1889i
2.4	0.7450	$\begin{bmatrix} 0.0128 & 0.1046 \\ -6.7244 & -1.7014 \end{bmatrix}$	-0.6671 -1.0215	$\begin{bmatrix} 0.0128 & 0.1038 \\ -6.7244 & -1.7008 \end{bmatrix}$	-0.6534 -1.0347

This section concludes that if the proportional gain is increased for tuning the system, bifurcation occurs for higher values of K_p. This leads to unwanted oscillations in the speed and current waveforms. This is confirmed by the phase plot presented in fig. 9 where period-1 and period-2 plots are depicted clearly.

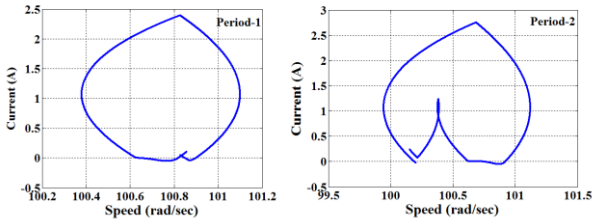

Fig 9. Phase plot for proportional gain variation (K_p=1.2 for period-1; K_p=2.4 for period-2)

Fig. 10 and 11 shows the speed and current waveforms for K_p=2.4 and 3.8 respectively. Without controller, when the proportional gain is increased, period doubling occurs at K_p=2.4. But with the use of ETDAS controller, period-1 is extended till K_p=3.8 and beyond that period-2 appears. If controller is not used, further increase in proportional gain beyond K_p=2.4 leads to chaos. Use of the controller extends the bifurcation to K_p=3.8. So normal period-1 behavior is extended to larger gain compared to the operation without controller. This improves the system performance if proportional gain is increased.

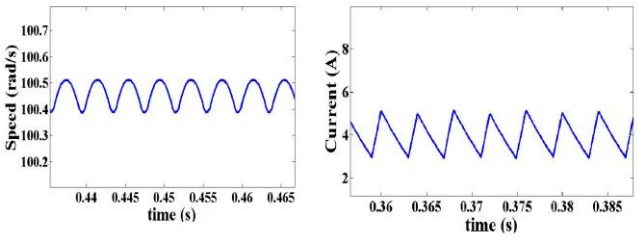

(a) (b)

Fig. 10. Speed and Current for K_p=2.4 with ETDAS controller

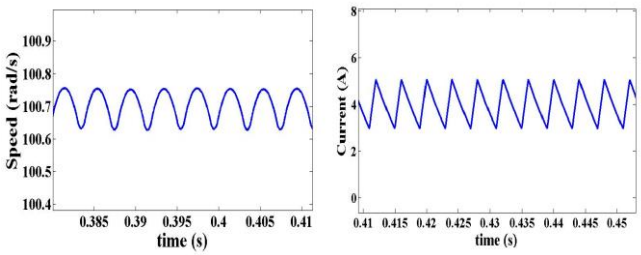

(a) (b)

Fig. 11. Speed and Current for K_p=3.8 with ETDAS controller

5.2 Effect of input voltage (V_{in}) on Eigen values

Now supply voltage is varied and the same behavior is observed. Speed of the motor is directly proportional to the supply voltage. It is necessary to change the supply voltage to control the speed of the motor. Table 3 shows the eigen values calculated for various supply voltages ranging from 85 V to 115 V.

Fig. 12 and Fig. 13 give the speed and current waveforms obtained for V_{in}=85 V and V_{in}=115 V from MATLAB simulink. When V_{in}=115 V, the system shows a period doubling bifurcation.

Because at this voltage, eigen values of both the matrices exceed unity in the negative real axis. The eigen value loci are presented in fig. 14. It is observed that the eigen values cross unity along the negative real axis in fig. 14(b).

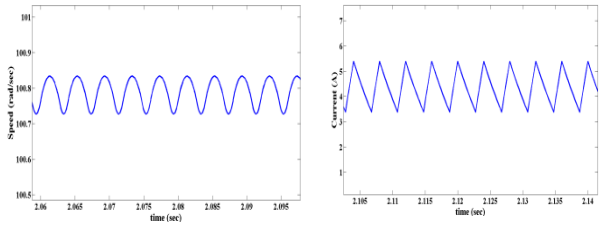

(a) (b)

Fig 12. Speed and Current output waveforms for T_L=0.39 Nm; V_{in}=85 V; R=3.5 Ω; K_p=2

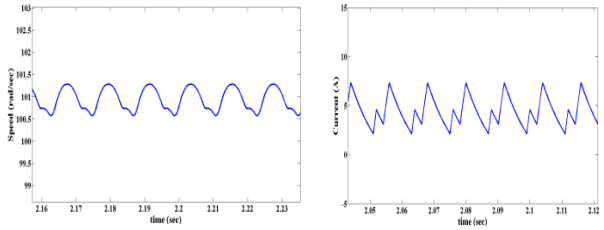

(a) (b)

Fig 13. Speed and Current output waveforms for T_L=0.39 Nm; V_{in}=115 V; R=3.5 Ω; K_p=2

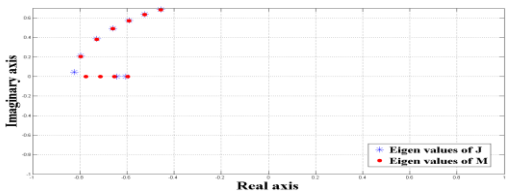

(a)

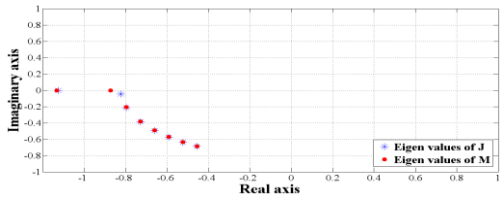

(b)

Fig 14. Comparisons of Eigen tracing for (a) speed and (b) current for various V_{in} values

Period doubling occurs if any one of the eigen values cross unity in the negative real axis. Phase plots confirm the normal and period doubling occurrence at V_{in}=85V and V_{in}=115V respectively as illustrated in fig. 15.

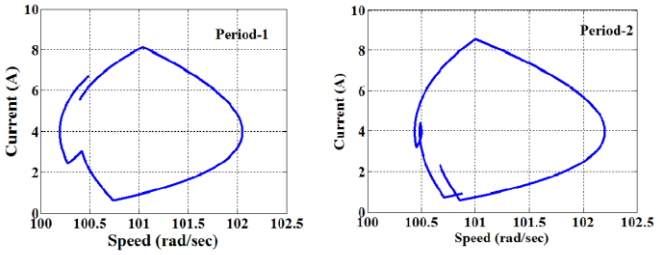

Fig 15. Phase plot for input voltage (V_{in}=85V for period-1;V_{in}=115V for period-2)

Speed control is essential for industrial drives based on the load requirement. In such case, supply voltage is controlled by means of adjusting PWM pulses. From the results obtained in this section, it is clear that if supply voltage is increased, it leads to bifurcation. This produces losses and unwanted errors if the motor drive is operating sensitive loads. If voltage is increased from 85V and at 115V period doubling occurs. If we increase further chaotic behavior arises causing unstable operation. But with the inclusion of ETDAS controller we can apply up to 200 V input voltage within period-1 operation. This means that period-1 operation appears till 200 V input voltage, the stable operation gets extended.

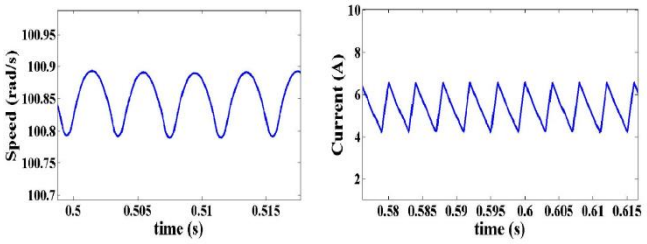

(a) (b)

Fig 16. Speed and Current for V_{in}=115 V with ETDAS controller

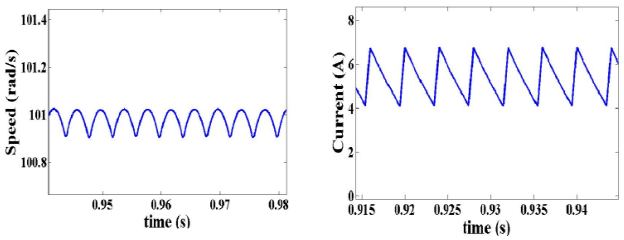

(a) (b)

Fig 17. Speed and Current for V_{in}=200 V with ETDAS controller

Table 3
Variation of supply voltage to find bifurcation

V_{in}	Δ	J Matrix	Eigen Values using Poincare map	M-matrix	Eigen values using Monodromy matrix
85	0.6998	$\begin{bmatrix} 0.1134 & 0.1567 \\ -5.0835 & -1.0254 \end{bmatrix}$	-0.4560 + 0.6874i -0.4560 - 0.6874i	$\begin{bmatrix} 0.1134 & 0.1559 \\ -5.0835 & -1.0248 \end{bmatrix}$	-0.4557 + 0.6844i -0.4557 - 0.6844i
90	0.7165	$\begin{bmatrix} 0.1158 & 0.1514 \\ -5.3855 & -1.1641 \end{bmatrix}$	-0.5241 + 0.6371i -0.5241 - 0.6371i	$\begin{bmatrix} 0.1158 & 0.1505 \\ -5.3855 & -1.1635 \end{bmatrix}$	-0.5239 + 0.6337i -0.5239 - 0.6337i
95	0.7313	$\begin{bmatrix} 0.1176 & 0.1466 \\ -5.6865 & -1.3019 \end{bmatrix}$	-0.5921 + 0.5745i -0.5921 - 0.5745i	$\begin{bmatrix} 0.1176 & 0.1458 \\ -5.6865 & -1.3014 \end{bmatrix}$	-0.5919 + 0.5707i -0.5919 - 0.5707i
100	0.7448	$\begin{bmatrix} 0.1197 & 0.1425 \\ -5.9887 & -1.4405 \end{bmatrix}$	-0.6604 + 0.4946i -0.6604 - 0.4946i	$\begin{bmatrix} 0.1196 & 0.1416 \\ -5.9887 & -1.4400 \end{bmatrix}$	-0.6602 + 0.4901i -0.6602 - 0.4901i
105	0.7569	$\begin{bmatrix} 0.1212 & 0.1387 \\ -6.2900 & -1.5784 \end{bmatrix}$	-0.7286 + 0.3874i -0.7286 - 0.3874i	$\begin{bmatrix} 0.1212 & 0.1379 \\ -6.2899 & -1.5778 \end{bmatrix}$	-0.7283 + 0.3815i -0.7283 - 0.3815i
115	0.7780	$\begin{bmatrix} 0.1241 & 0.1322 \\ -6.8928 & -1.8541 \end{bmatrix}$	-0.6058 -1.1242	$\begin{bmatrix} 0.1241 & 0.1314 \\ -6.8928 & -1.8536 \end{bmatrix}$	-0.5968 -1.1327

The speed and current waveforms for V_{in}=115V and 200V showing normal period-1 are shown in fig. 16 and 17 respectively. Period-2 is exhibited only after V_{in}=200 V. Thus the controller allows the larger supply voltage variation within stable operating limit.

5.3 Effect of Load torque on Eigen values

If variable load is applied to the motor drive under consideration, load torque can also be taken as the bifurcation parameter. In this subsection, load torque is decreased from 0.39 to 0.05 Nm and corresponding eigen values are calculated. The calculated eigen values are given in table 4. Since current is directly proportional to torque, decrease in torque decreases the armature current linearly. Fig. 18 and 19 shows the normal and bifurcation outputs obtained from Simulink model.

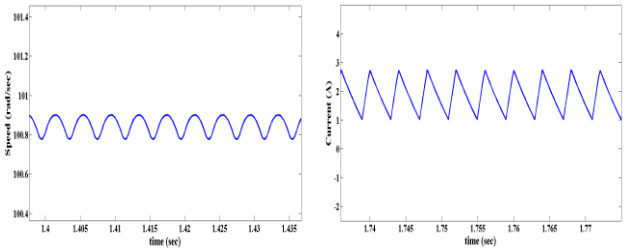

(a) (b)

Fig 18. Speed and Current output waveforms for T_L=0.2 Nm; V_{in}=80 V; R=3.5 Ω; K_p=2

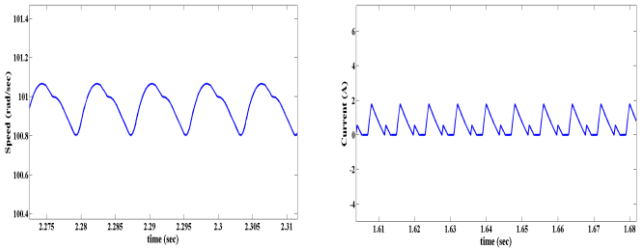

(a) (b)

Fig 19. Speed and Current output waveforms for T_L=0.02 Nm; V_{in}=80 V; R=3.5 Ω; K_p=2

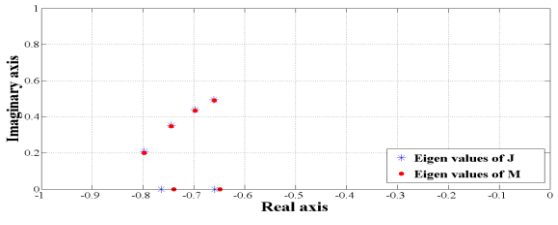

(a)

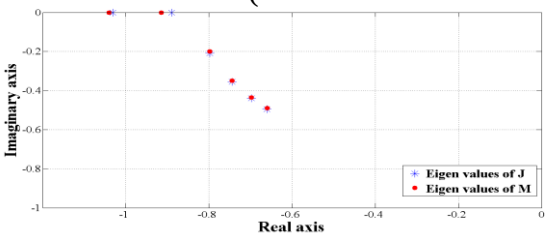

(b)

Fig 20. Comparisons of Eigen tracing for (a) speed and (b) current for various T_L values

Table 4
Variation of load torque to find bifurcation

T_L	δ	J Matrix	Eigen Values using Poincare map	M-matrix	Eigen values using Monodromy matrix
0.39	0.7451	$\begin{bmatrix} 0.1197 & 0.1425 \\ -5.9887 & -1.4405 \end{bmatrix}$	-0.6604 + 0.4946i -0.6604 - 0.4946i	$\begin{bmatrix} 0.1196 & 0.1416 \\ -5.9887 & -1.4400 \end{bmatrix}$	-0.6602 + 0.4901i -0.6602 - 0.4901i
0.3	0.7685	$\begin{bmatrix} 0.1775 & 0.1550 \\ -6.1937 & -1.5732 \end{bmatrix}$	-0.6979 + 0.4400i -0.6979 - 0.4400i	$\begin{bmatrix} 0.1775 & 0.1542 \\ -6.1937 & -1.5727 \end{bmatrix}$	-0.6976 + 0.4351i -0.6976 - 0.4351i
0.2	0.795	$\begin{bmatrix} 0.2452 & 0.1715 \\ -6.4475 & -1.7349 \end{bmatrix}$	-0.7448 + 0.3544i -0.7448 - 0.3544i	$\begin{bmatrix} 0.2452 & 0.1708 \\ -6.4474 & -1.7344 \end{bmatrix}$	-0.7446 + 0.3486i -0.7446 - 0.3486i
0.1	0.8214	$\begin{bmatrix} 0.3166 & 0.1910 \\ -6.7301 & -1.9122 \end{bmatrix}$	-0.7978 + 0.2087i -0.7978 - 0.2087i	$\begin{bmatrix} 0.3165 & 0.1903 \\ -6.7301 & -1.9118 \end{bmatrix}$	-0.7976 + 0.1992i -0.7976 - 0.1992i
0.05	0.8346	$\begin{bmatrix} 0.3539 & 0.2020 \\ -6.8841 & -2.0079 \end{bmatrix}$	-0.7640 -0.8900	$\begin{bmatrix} 0.3539 & 0.2014 \\ -6.8841 & -2.0075 \end{bmatrix}$	-0.7392 -0.9144
0.02	0.8425	$\begin{bmatrix} 0.3769 & 0.2090 \\ -6.9807 & -2.0675 \end{bmatrix}$	-0.6589 -1.0318	$\begin{bmatrix} 0.3769 & 0.2084 \\ -6.9807 & -2.0672 \end{bmatrix}$	-0.6492 -1.0411

Fig. 20 illustrates the eigen value plot for various load torques. At a magnitude of 0.05 Nm load torque, one of the eigen values cross unit circle showing bifurcated eigen value locus. Fig. 20 (a) shows the eigen values for speed state vector and fig. 20 (b) shows the eigen values for current state vector. The unity crossing in the negative real axis confirms the occurrence of period doubling bifurcation.

Fig 21. Phase plot for load torque variation (T_L=0.2 Nm for period-1, T_L=0.02 for period-2)

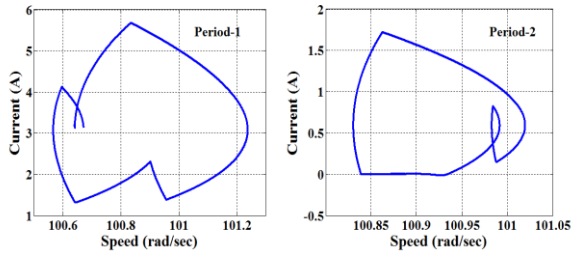

The same behavior can be clearly shown in the phase plot presented by fig. 21 also. It is inferred that when the motor is lightly loaded, load torque gets reduced which leads to bifurcation. If we reduce the torque from 0.39 to 0.02 Nm, flip bifurcation occurs. Introduction of controller produces period-1 operation even for 0.01 Nm. These behaviors can be visualized in the simulation waveforms presented in fig. 22 and 23.

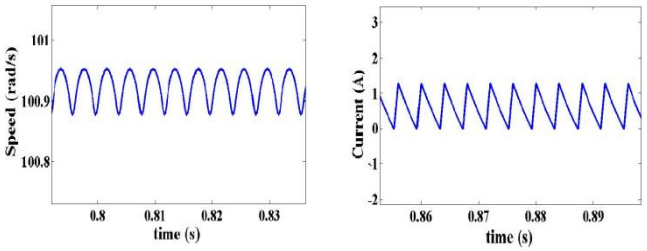

(a) (b)

Fig 22. Speed and Current for T_L=0.01 Nm with ETDAS controller

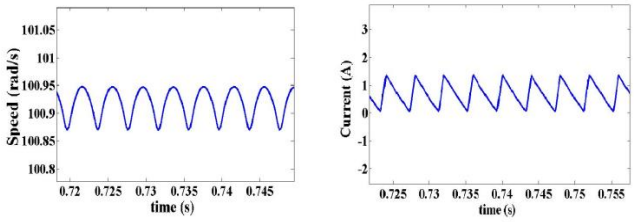

(a) (b)

Fig 23. Speed and Current for T_L=0.02 Nm with ETDAS controller

So the performance of the motor is improved and normal operation gets extended. If the motor is used in specified application performing parameter variation, chaos can be avoided for larger variation of parameter. Thus the system becomes reliable and efficient.

From the above results, it is possible to find the stable operating parametric condition of the PMDC motor drive system. If the motor drive is

operated in this stable region, performance can be improved. Though chaos cannot be predicted, it can be extended by properly including the controller in the system. This work can be extended to identify the period doubling bifurcation with some other parameter variation. Also control techniques like Fuzzy logic, ANN, ANFIS or some other evolutionary algorithms can be applied to control bifurcation and extend the stable operation.

6. Conclusion

In this paper, chaos present in the PMDC drive is analyzed using both Poincare mapping and Monodromy matrix methods. The analysis is based on the Eigen values of the system Jacobian and Monodromy matrix. Closed loop control of the motor drive is taken for the analysis and the methodology used are derived in detail. Eigen values are tabulated for different parametric conditions for comparison of the two methods. Though these two methods identify the nature of the system, there is a small difference in the point of bifurcation. It shows the sensitivity of the system and this analysis is useful in determining the stable operating region of the system. Further this calculation is verified using MATLAB Simulink with the same parameter values. The simulation results confirm with the tabulated Eigen values. A graphical representation of Eigen values is also presented in the form of Eigen value plot. If the motor drive is operated in the stable parameter range, occurrence of chaos can be eliminated. Though these two methods involve in different procedure for calculating the Eigen values, the results obtained are approximately same. An ETDAS controller is incorporated in the system to extend the normal period-1 operation of the drive under parameter variations. The speed and current waveforms of the drive after the inclusion of controller is also presented. All the results and graphs shown are used for finding the stable operating points of the system. This gives us clear information about the stable operating region of the system and it is possible to avoid chaos.

References

[1] Nagy,I: *Nonlinear phenomena in power electronics.* In:J.Automatika,Vol.42,No.3/4,2001,p.117-132.

[2] Tucker, W. *Computing accurate Poincare maps*.In: Physica D: Nonlinear Phenomena, Vol.171,No. 3, 2002,p.127-137.

[3] Chau, K. T., Chen, J. H.Chan, C. C.: *Modeling of subharmonics and chaos in DC motor drives*. In:28th Annual IEEE Power Electronics Specialists Conf (1997),Vol.2, June 21-27, 1997, p.1330-1336,St Louis, MO.

[4] Dai, D., Ma, X., Zhang, B.,Tse Chi, K.: *Hopf Bifurcation and chaos from torus breakdown in voltage-mode controlled DC drive systems*.In: Chaos, Solitons& Fractals,Vol.4, No.2,2009, p.1027-1033.

[5] Chen, J. H., Chau, K.T.,Chan C. C.: *Analysis of chaos in current-mode-controlled DC drive systems*. In:IEEE Trans.Industrial Electronics, Vol.47,No.1, 2000, p.67-76.

[6] Okafor, N., Zahawi, B., Giaouris, D., Banerjee, S.: *Chaos, coexisting attractors, and fractal basin boundaries in DC drives with full-bridge converter*.In: *Proc. IEEE Int. Sym. Circuits and Systems*(2010), May 30-June 2, 2010, p.129-132,Paris, France.

[7] Tang, T., Yang, M., Li, H. Shen, D.:*A new discovery and analysis on chaos and bifurcation in dc motor drive system with full-bridge converter*.In: IEEEInt. Conf. Industrial Electronics and Applications (2006), May 24-26, 2006, pp. 1-6,Singapore.

[8] Wang, Z., &Chau, K. T. :*Anti-control of chaos of a permanent magnet DC motor system for vibratory compactors*.In: Chaos, Solitons& Fractals,Vol.36, No.3,2008,p.694-708.

[9] Chau, K. T., Chen, J. H., Chan, C. C., Chan, D.T.W. :*Modeling of subharmonics and chaos in DC motor drives*. In:23rd Int. Conf. Industrial Electronics, Control and Instrumentation(1997), November 09-14, 1997, p. 523-528,New Orleans, LA.

[10] Yildiz, A.B.:*Electrical equivalent circuit based modeling and analysis of direct current motors*. In: Int. J. of Electrical Power & Energy Systems,Vol.43,No.1, 2012,p.1043-1047.

[11] Chen, J.H., Chau, K.T., Chan, C.C., Jiang, Q.: *Subharmonics and chaos in switched reluctance motor drives.*In:IEEE Trans. Energy Conversion,Vol.17,No.1, 2002,p.73-78.

[12] Chang, S.C., Lin, H.P.: *Chaos attitude motion and chaos control in an automotive wiper system*. In:Int. J. of solids and structures,Vol.41,No.13,2004, p.3491-3504.

[13] Ge, Z.M. & Cheng, J.W. :*Chaos synchronization and parameter identification of three time scales brushless DC motor system*.In: Chaos, Solitons& Fractals,Vol.24, No.2, p.597-616.

[14] Haipeng, Ding Liu :*Nonlinear feedback control of chaos in permanent magnet synchronous motor*. In: IEEE Transactions on Circuits and Systems II: Express Briefs, Vol.53, No.1, 2006,p.45-50.

[15] Wang, Z., Chau, K. T.:*Control of chaotic vibration in automotive wiper systems*. In: Chaos, Solitons& Fractals,Vol.39,No.1, p.168-181.

[16] Okafor, N.C.:*Analysis and control of nonlinear phenomena in electrical drives* . Ph.D thesis, Newcastle University, UK, 2012.

[17] Ge, Zheng-Ming, Ching-Ming Chang, Yen-Sheng Chen: *Anti-control of chaos of single time scale brushless dc motors and chaos synchronization of different order systems*. In: Chaos, Solitons& Fractals, Vol.27, No.5,2006,p.1298-1315.

[18] Harb, Ahmad, M.: *Nonlinear chaos control in a permanent magnet reluctance machine*. In:Chaos, Solitons& Fractals,Vol.19, No.5,2004, p.1217-1224.

[19] Ge,Z.M., Lee, C.I.: *Control, anticontrol and synchronization of chaos for an autonomous rotational machine system with time-delay*. In: Chaos, Solitons& Fractals, Vol.23, No.5, 2005, p.1855-1864.

[20] Li, Chun-Lai, Wen Li, Fu-Dong Li :*Chaos induced in Brushless DC Motor via current time-delayed feedback.* In: Optik-International Journal for Light and Electron Optics, Vol.125, No. 21,2014,p.6589-6593.